Inorganic Chemistry

Article

pubs.acs.org/IC

Mass Spectrometric and Computational Investigation of the Protonated Carnosine−Carboplatin Complex Fragmentation

Ida Ritacco,[†] Emilia Sicilia,*[,†] Tamer Shoeib,*[,‡,§] Mohamed Korany,[‡] and Nino Russo[†]

[†]Dipartimento di Chimica e Tecnologie Chmiche, Università della Calabria, I-87036 Arcavacata di Rende, Italy

[‡]Department of Chemistry, The American University in Cairo, New Cairo 11835, Egypt

[§]Centre for Analytical Science, Department of Chemistry, Loughborough University, Loughborough, Leicestershire LE11 3TU, U.K.

Supporting Information

ABSTRACT: Platinum(II)-based anticancer drugs are square-planar d^8 complexes that, activated by hydrolysis, cause cancer cell death by binding to nuclear DNA and distorting its structure. For that reason, interactions of platinum anticancer drugs with DNA have been extensively investigated, aiming at disentangling the mechanism of action and toxicity. Less attention, however, has been devoted to the formation of adducts between platinum drugs with biological ligands other than DNA. These adducts can cause the loss and deactivation of the drug before it arrives at the ultimate target and are also thought to contribute to the drug's toxicity. Here are reported the outcomes of electrospray ionization mass spectrometry experiments and density functional theory (DFT) computations carried out to investigate the fragmentation pathways of the protonated carnosine−carboplatin complex, $[Carnosine + CarbPt + H]^+$. DFT calculations at the B3LYP/LANL2DZ level employed to probe fragmentation mechanisms account for all experimental data. Because of the relative rigidity of the structure of the most stable **1A** conformer, stabilized by three strong hydrogen bonds, the first step of all of the examined fragmentation pathways is the interconversion of the **1A** conformer into the less stable structure **1B**. Formation of the $[Carnosine + H]^+$ fragment from the precursor ion, $[Carnosine + CarbPt + H]^+$, is calculated to be the lowest-energy process. At slightly higher energies, the loss of two amino groups is observed to produce the $[Carnosine + (CarbPt - NH_3) + H]^+$ and $[Carnosine + (CarbPt - 2NH_3) + H]^+$ ions. At significantly higher energies, the loss of CO_2 occurs, yielding the final $[Carnosine + (CarbPt - NH_3) - CO_2 + H]^+$ and $[Carnosine + (CarbPt - 2NH_3) - CO_2 + H]^+$ products. Formation of the $[CarbPt + H]^+$ fragment from $[Carnosine + CarbPt + H]^+$, even if not hampered by a high activation barrier, is calculated to be very unfavorable from a thermodynamic point of view.

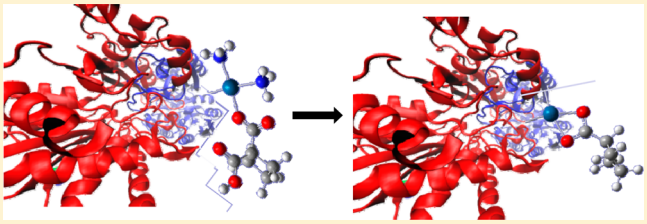

1. INTRODUCTION

Cisplatin [*cis*-diamminedichloroplatinum(II)] is the first inorganic compound introduced in clinical use for the treatment of cancer.[1−4] It is a prototype of several platinum[5−8] and other metal[9−12] coordination compounds synthesized and tested in the search for novel cytostatic agents with improved therapeutic characteristics with respect to the parent compound. Today, the most common platinum(II)-based anticancer drugs used worldwide are cisplatin, carboplatin, and oxaliplatin. These are square-planar d^8 platinum(II) complexes causing cancer cell death by binding to nuclear DNA and distorting its structure.[13,14] Carboplatin [*cis*-diammine-(cyclobutane-1,1-dicarboxylato)platinum(II)] is a platinum anticancer drug used for the treatment of many types of human cancer. Carboplatin was developed by Rosenberg and colleagues in the early 1970s to improve the clinical performance of the first-generation platinum anticancer drug cisplatin[15,16] Carboplatin has been found to be much less oto-, neuro-, and nephrotoxic than cisplatin.[17,18] Carboplatin contains a structural feature that makes the compound much less chemically reactive than cisplatin, that is a bidentate dicarboxylate chelate leaving ligand.[18] The range of measured values of the pseudo-first-order rate constant for the first hydrolysis reaction of carboplatin, a reaction involving the displacement of one "arm" of the cyclobutane-1,1-dicarboxylate (CBDCA) chelate ring from the Pt^{2+} ion by a water molecule, is unusually wide.[19−21] There is also an analogous discrepancy in the reported rate constant for the displacement of one of the chloro ligands of cisplatin by water.[21,22] Despite this, however, the fact that the rate constant for the hydrolysis of carboplatin is about 2 orders of magnitude smaller than the corresponding hydrolysis rate for cisplatin has encouraged investigations focused on possible activation mechanisms of carboplatin in chemotherapy. Interactions of platinum anticancer drugs with DNA to understand the mechanism of action and toxicity have been extensively investigated,[17,23−25] whereas less attention has been devoted to the undesirable interactions of platinum drugs with biological ligands other than DNA that can cause the loss and deactivation of the drug before it arrives at the ultimate target.

Received: April 28, 2015
Published: August 4, 2015

DOI: 10.1021/acs.inorgchem.5b00959
Inorg. Chem. 2015, 54, 7885−7897

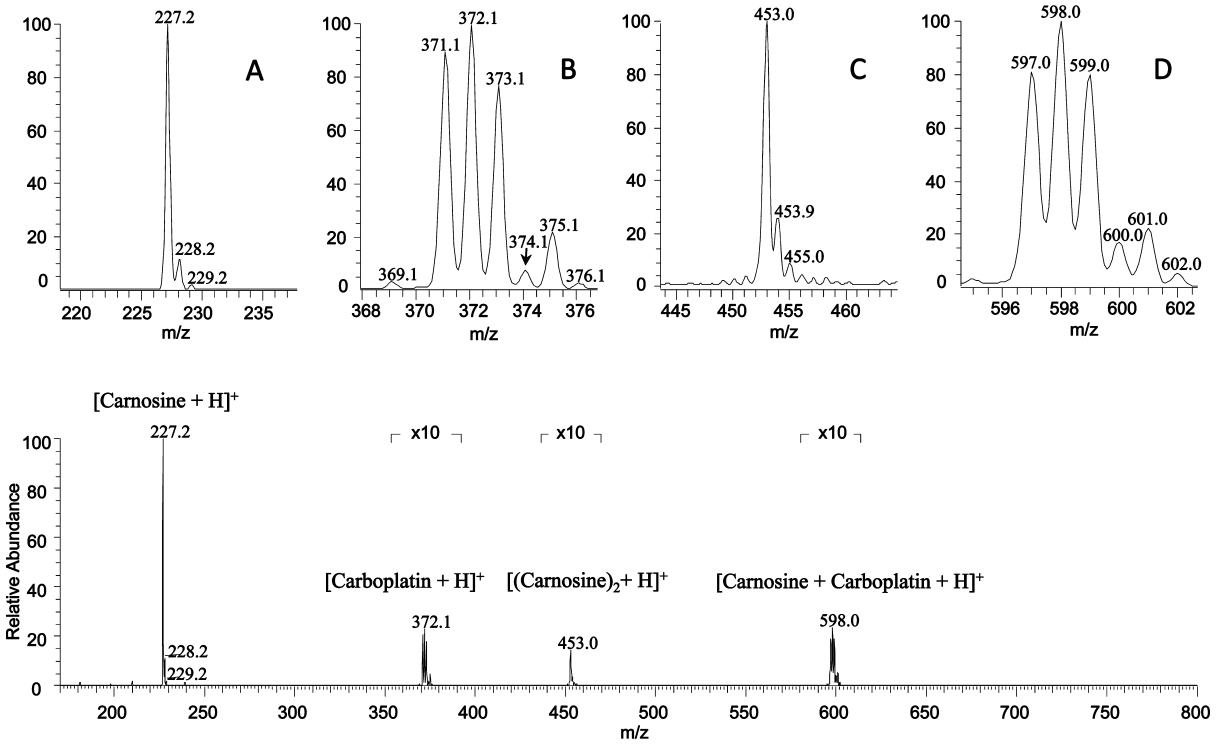

Figure 1. Full-Scan MS spectrum of a 2:1 molar ratio mixture of camosine and carboplatin in a 1:1 (v/v) water−mefhanol solution as obtained on the LTQ without allowing for the incubation time. The sections of the spectrum shown under "×10" signify the magnification of the signal by 10-fold for clarity. This magnification means that, for example, the intensity of the ion at m/z 453.0 is about 2% of the base peak. The signals assigned to $[\text{Camosine} + \text{H}]^+$, $[\text{Carboplatin} - \text{H}]^+$, $[(\text{Camosine})_2 + \text{H}]^+$, and $[\text{Camosine} + \text{Carboplatin} + \text{H}]^+$ are each expanded and normalized to 100% in insets A−D, respectively, for clarity.

The dipeptide β-alanine-L-histidine, commonly known as carnosine, is a naturally occurring substance synthesized by endogenous carnosine synthetase. It is present at elevated levels in human skeletal and cardiac muscles as well as in brain tissue[26−30] and is typically concentrated in the cytosol of cells due to its water solubility.[31] Several possible physiological function roles have been considered since its first discovery[32,33] such as pH buffering,[34] metal chelation,[35] or neurotransmitter function.[36] Carnosine is also reported to have antioxidant activity because of its ability to react with several highly reactive species, such as hydroxyl, super oxide, and molecular oxygen free radicals, especially in the water-rich environment inside the body.[37] More recently, it has also been shown that carnosine can play a role in complexation with and sequestering of platinum anticancer drugs.[38] In vitro studies on hepatocellular carcinoma HepG2 cells have shown that carnosine may inhibit the cytotoxic action of oxaliplatin, most likely through the formation of complexes that are less cytotoxic than oxaliplatin alone.[38] The interaction between oxaliplatin and carnosine has been the subject of a recent study.[39] In this study, we offer the results of a joint theoretical and experimental study of the interactions between carboplatin and carnosine including a detailed description of the fragmentation pathways for the gas-phase dissociation of the protonated carboplatin−carnosine complex. Calculated potential energy surfaces (PESs) for the dissociation processes are compared with collision-induced dissociation (CID) experiments. Such studies are important not only to better understand the mechanism of action and toxicity of platinum anticancer drugs but also for the optimization and design of new and improved platinum-based antineoplastic agents.

2. EXPERIMENTAL SECTION

Instrumentation. An LTQ linear-ion-trap mass spectrometer with an electrospray source and a high-resolution Q-Exactive Fourier transform mass spectrometer (Thermo Electron, San Jose, CA) were used. Both instruments were calibrated using Ultramark 1621, caffeine, and Met-Arg-Phe-Ala in accordance with the manufacturer's recommendations. The Q-Exactive was equipped with a Tri-Versa NanoMate ESI chip nanospray (Advion, New York, NY). Typical resolving powers obtained from the Q-Exactive for the mass range under study were on the order of 60000. For the LTQ, resolving powers achieved were on the order of 1500, while the upper instrumental error limit in measurements was 0.2 m/z units. The LTQ autotune routine was used to obtain lens, quadrupole, and octapole voltages for maximum transmission of the ions of interest. Helium gas, admitted into the ion trap at a maintained pressure of approximately 10^{-3} torr, was used as the buffer gas to improve the trapping efficiency and as the collision gas for CID experiments performed here. Experiments designed to elucidate ion structures or fragmentation pathways on the LTQ were performed as follows: the entire isotopic envelope of the ion of interest was selected by having an isolation width set to 5 m/z units and then collisionally activated by setting the activation amplitude at 25−35% of the maximum voltage available (determined empirically), and the activation Q setting (used to adjust the frequency of the radio-frequency excitation voltage) was set at 0.25 units. Sample solutions were continuously infused at a flow rate of 5 μL min^{-1} into the pneumatically assisted electrospray probe using dry nitrogen as the nebulizing gas. Auxiliary and sheath gases were tuned daily for maximum signal transmission. The experiments reported here were all performed under multiple-collision conditions.

Reagents. Carnosine, carboplatin, HPLC-grade water, and methanol were all purchased from Sigma-Aldrich, U.K.

Computational Methods. All molecular geometries have been optimized without any geometrical constraint in the framework of the density functional theory (DFT) that is based upon a strategy of

DOI: 10.1021/acs.inorgchem.5b00959
Inorg. Chem. 2015, 54, 7885−7897

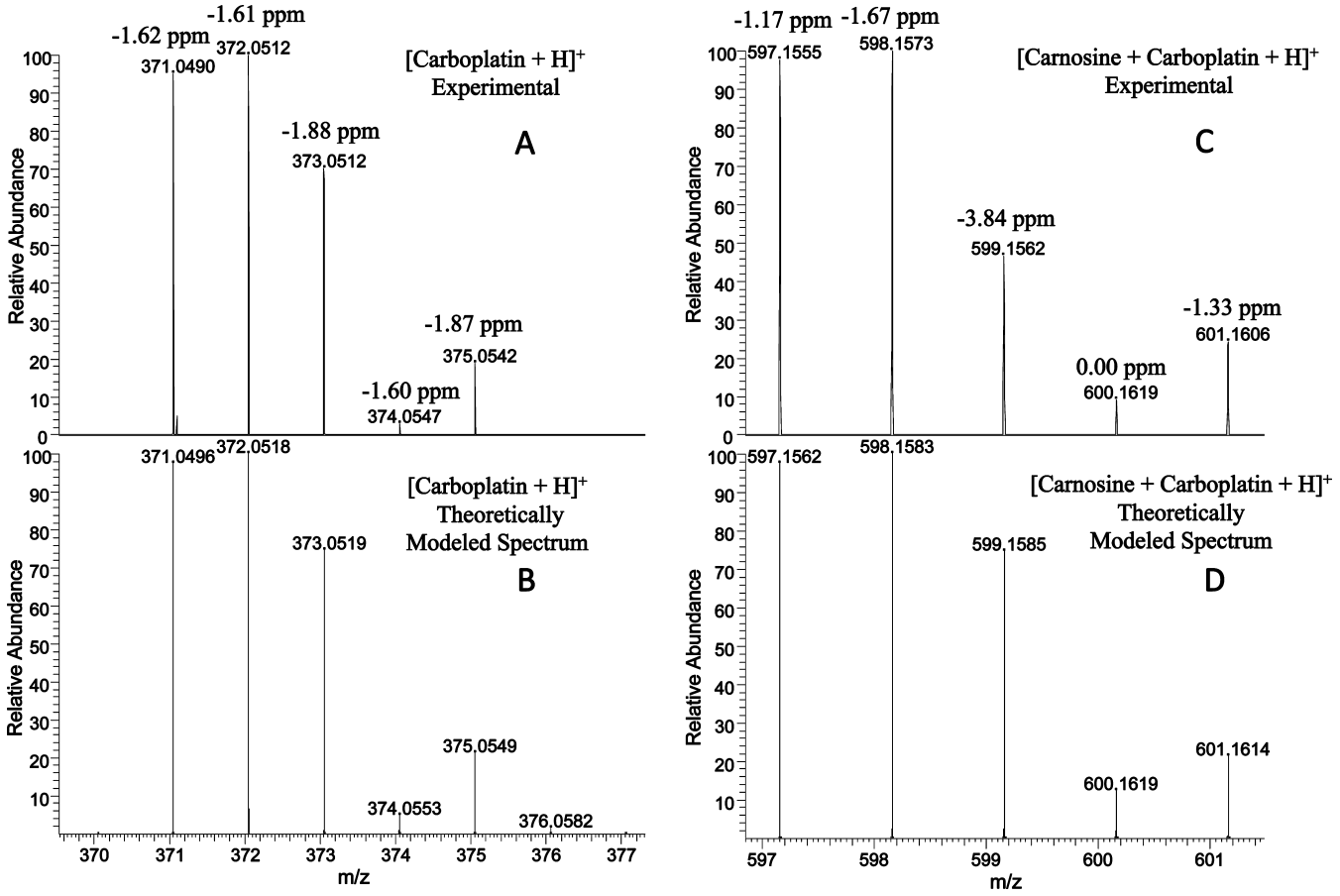

Figure 2. Full-scan MS spectrum of a 2:1 molar ratio mixture of camosine and carboplatin in a 1:1 (v/v) water−methanol solution as obtained on the Q-Exactive FT-MS without allowing for the incubation time. The experimental signals assigned to $[Carboplatin + H]^+$ and $[Camosine + Carboplatin + H]^+$ are each expanded and normalized to 100% in insets A and C, respectively, and insets B and D show the theoretically modeled spectra for $[Carboplatin + H]^+$ and $[Camosine + Carboplatin + H]^+$, respectively, using the *Thermo Xcalibur* software. Errors (in ppm) are listed next to each experimental isotopic peak observed.

modeling electron correlation via the proper functionals of the electron density. The B3LYP Becke's three-parameter exchange-correlation hybrid functional with nonlocal correlation corrections, provided by Lee, Yang, and Parr, has been used in the calculations.[40−42] The LANL2DZ basis sets of Hay and Wadt have been employed for all atoms.[43−45] The successful use of the B3LYP/LANL2DZ computational protocol for the investigation of both the electronic properties and reaction pathways of transition-metal-containing compounds, including anticancer drugs, is well established.[46−57] The same protocol has been proven, recently, to give reliable results in the investigation of the fragmentation pathways of the oxaliplatin−carnosine complex.[58] Frequency calculations at the same level of theory have also been performed to identify all stationary points as minima (zero imaginary frequencies) or transition states (one imaginary frequency). The vibrational mode associated with the imaginary frequency of each intercepted transition state has been shown to correspond to the correct movement of the involved atoms. Moreover, the involved transition states have been checked by intrinsic-reaction-coordinate analysis to show the proper connection to the corresponding minima.[59,60] All of the calculations have been performed with the *Gaussian 09* software package.[61]

3. RESULTS AND DISCUSSION

Figure 1 shows the electrospray ionization mass spectrometry (ESI-MS) full-scan spectrum of a 2:1 mM solution in each of carnosine and carboplatin dissolved in a 1:1 (v/v) deionized water−methanol mixture. This figure shows a base peak at m/z 227 corresponding to protonated carnosine, $[Carnosine + H]^+$. The peak at m/z 453 and the two clusters around m/z 372 and 598 are assigned to the protonated carnosine dimer, $[(Carnosine)_2 + H]+$, protonated carboplatin, $[CarbPt + H]^+$, and protonated carnosine−carboplatin complex, $[Car + CarbPt + H]^+$, respectively.

The assignments of these ions have been confirmed by comparing the observed isotopic patterns to those theoretically modeled for each of the proposed species. For further confirmation, the isotopic patterns for the proposed $[Carboplatin + H]^+$ and $[Carnosine + Carboplatin + H]^+$ species, where the latter is the focus of this study, have been obtained on the Q-Exactive FT-MS at a resolving power of about 60000 and compared to their theoretical isotopic patterns at an equivalent resolution. The average errors obtained over all of the isotopic peaks observed were 1.72 and 1.60 ppm for $[Carboplatin + H]^+$ and $[Carnosine + Carboplatin + H]^+$, respectively. This mass accuracy, being below the commonly accepted 2 ppm limit and obtained without the use of lock masses, provided unequivocal identifications, as seen in Figure 2.

The mass selection and subsequent CID of the entire isotopic envelope of the ion $[Carnosine + CarbPt + H]^+$ resulted in the MS^2 spectrum shown in Figure 3. As was previously reported in the fragmentation of other platinum drug complexes to carnosine,[58,38] here there is also no difference in the fragmentation pathway of the $[Carnosine +$

DOI: 10.1021/acs.inorgchem.5b00959
Inorg. Chem. 2015, 54, 7885−7897

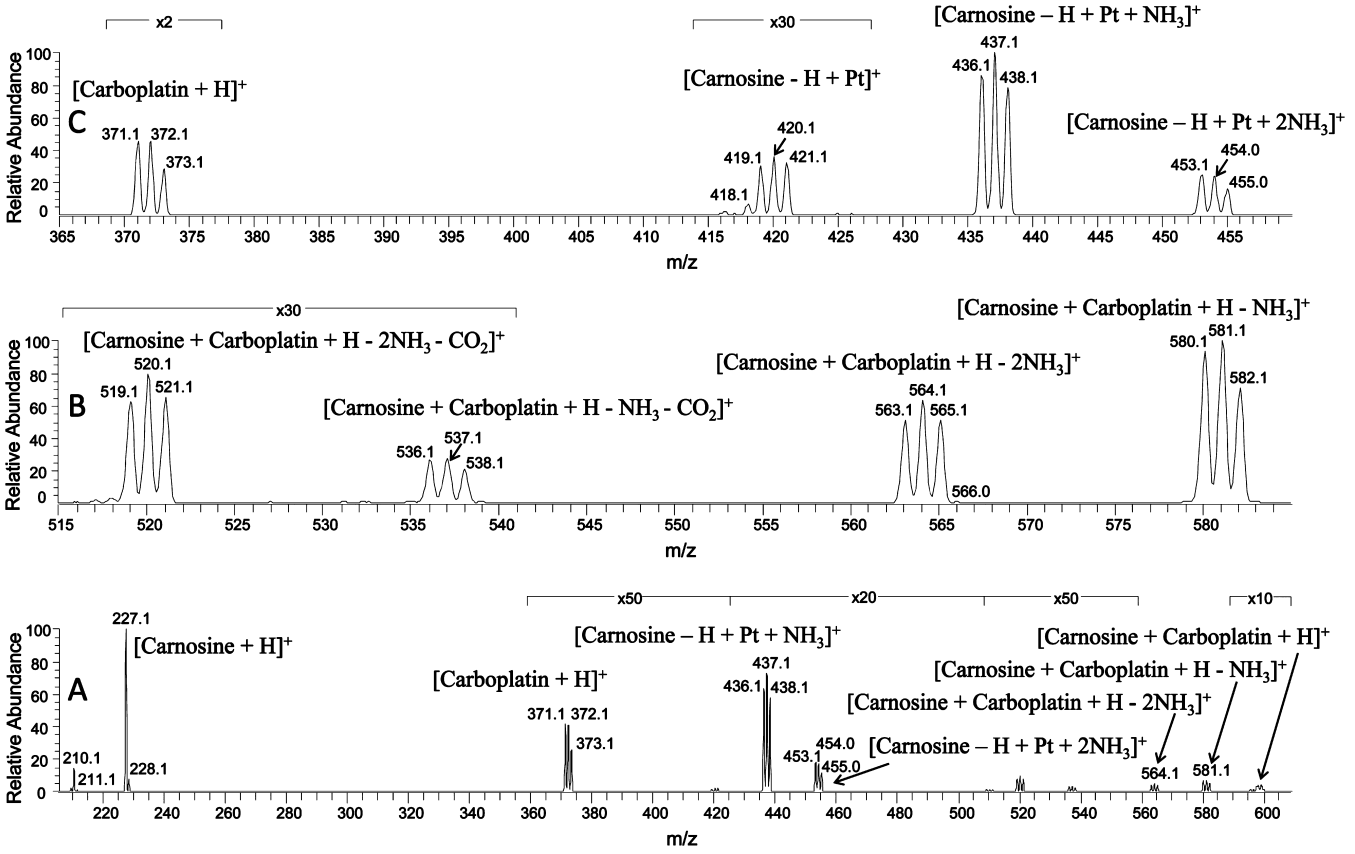

Figure 3. (A) Full scan MS^2 spectrum of the entire isotopic envelope of the ion [Camosine + Carboplatin + H]$^+$ generated at 15 eV in the laboratory frame and isolated from a (2:1) molar mixture of Camosine and Caboplatin in a (1:1) (v/v) water–methanol solution as obtained on the LTQ without allowing for the incubation time. (B and C) m/z 515–585 and 365–460 regions that are each expanded and normalized to 100%, respectively, for clarity.

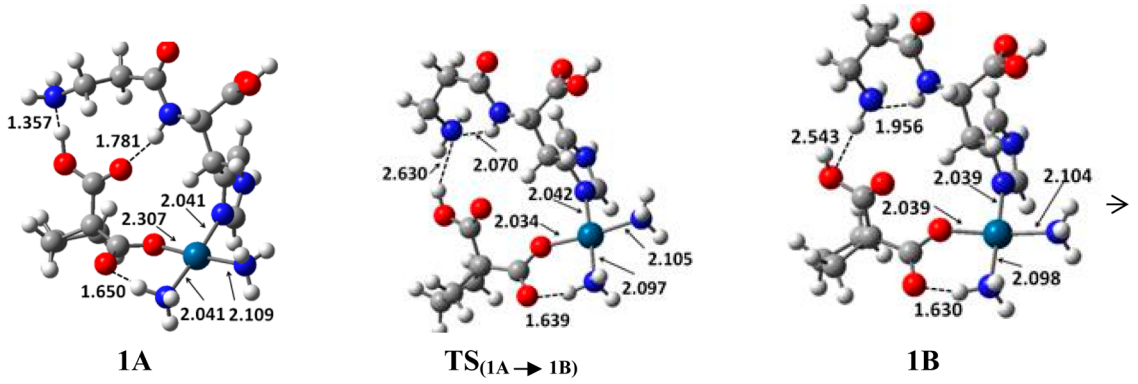

Figure 4. Geometrical structures of stationary points for the starting rearrangement of the most stable conformer **1A** into the less stable **1B** one through the $\mathbf{TS}_{(1A \rightarrow 1B)}$ transition state. Bond lengths are in angstroms. Gray, red, blue, and white spheres represent carbon, oxygen, nitrogen, and hydrogen atoms, respectively.

CarbPt + H]$^+$ complex among the different platinum isotopes. The generated product ion clusters centered around m/z 581, 564, 537, 520, 454, 437, 420, and 372 have been assigned as [Carnosine + CarbPt − NH_3 + H]$^+$, [Carnosine + CarbPt − $2NH_3$ + H]$^+$, [Carnosine + CarbPt − NH_3 − CO_2 + H]$^+$, [Carnosine + CarbPt − $2NH_3$ − CO_2 + H]$^+$, [Carnosine − H + $Pt(NH_3)_2$]$^+$, [Carnosine − H + $Pt(NH_3)$]$^+$, [Carnosine − H + Pt]$^+$, and [Carb + H]$^+$, respectively. Fragmentation pathways for the [Carnosine + CarbPt + H]$^+$ complex, leading to the experimentally determined product ions, have been theoretically investigated.

All of the reported pathways start with the structural rearrangement of the most stable conformer, labeled **1A**, of the precursor ion [Carnosine + CarbPt + H]$^+$ observed as the ion cluster around m/z 598, into conformer **1B**, being 14.0 kcal mol^{-1} higher in energy. The structures of these two minima and transition state $\mathbf{TS}_{(1A \rightarrow 1B)}$ allowing their interconversion are shown in Figure 4. Cartesian coordinates can be found (see Table S1) in the Supporting Information (SI).

It has been previously shown[55] that 46 conformers of the [Carnosine + CarbPt + H]$^+$ complex have been found to exist in a range of about 25 kcal mol^{-1}. These calculated structures

DOI: 10.1021/acs.inorgchem.5b00959
Inorg. Chem. 2015, 54, 7885–7897

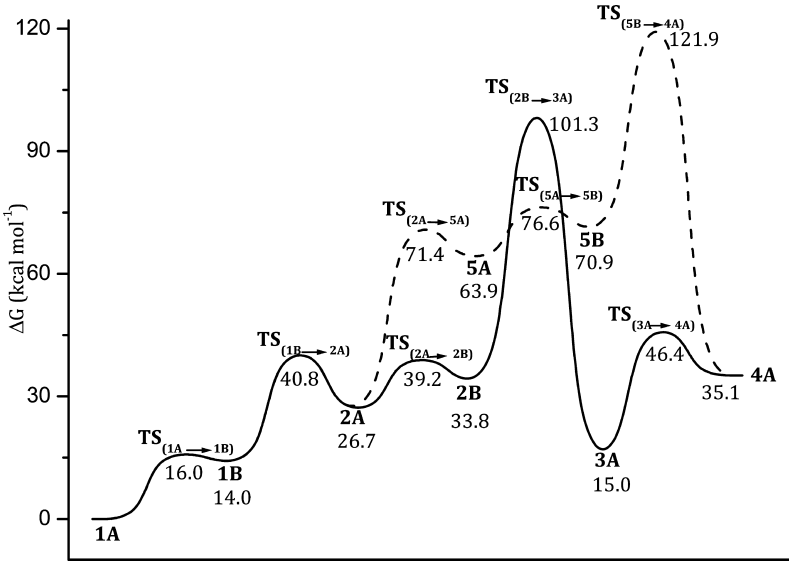

Figure 5. PES for fragmentation of the protonated carnosine−carboplatin complex: ion **1A** along pathways 1 (dashed line) and 2 (solid line). Structure labels are in bold; relative free energies are in kcal mol^{-1}.

involved either direct platinum bonding to carnosine or electrostatic interactions between protonated carnosine and CarbPt. In this figure, structure **1A** shows one of the Pt−O bonds of the CBDCA ligand to be substituted by a formal platinum coordination to the electron-rich *pros* imidazole nitrogen on the carnosine substrate. This structure is further stabilized by three hydrogen bonds. One of these is between one of the hydrogen atoms of the NH_3 group on platinum and the oxygen atom of one carboxylic group of the CBDCA moiety, forming a pseudo six-membered ring, another is between the hydrogen atom of the amide group and the oxygen atom of the other carboxyl group of CBDCA, and the third is between the nitrogen atom of the terminal amino group and the hydrogen atom of one of the carboxylic groups of CBDCA at 1.650, 1.781, and 1.357 Å, respectively. The number and strength of such hydrogen bonds make structure **1A** a relatively rigid conformer, and the rearrangement to **1B** is therefore required to allow for further fragmentation. The interconversion of structure **1A** into **1B** slightly shortens the length of the hydrogen bond between the amino group and the carboxyl group of CBDCA at 1.630 Å, whereas the hydrogen bond between the nitrogen atom of the terminal amino group and the OH group is no longer present. On the other hand, the bond between the nitrogen atom of the amide moiety and the other carboxyl group of CBDCA is substituted by a new hydrogen bond, at 1.956 Å, between the amide nitrogen atom and the terminal amino group. The rearrangement occurs, as shown in Figures 4 and 5, by overcoming a free-energy barrier of 16 kcal mol^{-1} for the transition state $\mathbf{TS_{(1A\rightarrow 1B)}}$ and leads to formation of the **1B** minimum lying 14 kcal mol^{-1} above the reference energy of **1A**. The breaking of one hydrogen bond and formation of a new weaker one are partially responsible for the calculated destabilization. The fragmentation of $[\text{Carnosine} + \text{CarbPt} + H]^+$ proceeds by the loss of neutral ammonia from structure **1B** to give the fragment ion $[\text{Carnosine} + (\text{CarbPt} - NH_3) + H]^+$ observed as the ion cluster centered around m/z 581. Either the NH_3 molecules in the trans position to the CBDCA moiety of carboplatin or those in the cis position can be eliminated. Following elimination of the first NH_3 molecule, either the fragmentation continues with elimination of the second carboplatin NH_3 molecule preceding elimination of CO_2 from the COOH unit of the CBDCA moiety or elimination of the CO_2 molecule may take place before elimination of the second NH_3 molecule. The peak at m/z 372 indicates that the fragment $[\text{CarbPt} + H]^+$ is formed from the precursor ion $[\text{Carnosine} + \text{CarbPt} + H]^+$ due to the loss of neutral carnosine.

Fragmentation Pathways 1 and 2: Elimination of the NH_3 Molecule Cis to the CBDCA Ligand. After rearrangement of the **1A** conformer to **1B**, elimination of the NH_3 molecule cis to the CBDCA moiety of carboplatin leads to formation of the fragment ion $[\text{Carnosine} + (\text{CarbPt} - NH_3) + H]^+$ observed as the ion cluster centered around m/z 581. Calculated free-energy profiles starting with elimination of the NH_3 molecule cis to the CBDCA moiety are depicted in Figure 5. Structure **2A** shows the initial step in the release of the NH_3 molecule cis to the CBDC moiety of carboplatin, with all other minima resulting from its subsequent dissociation, and the transition states leading to their formation are sketched in Figure 6. More detailed information on the geometrical parameters and Cartesian coordinates is reported in the SI (Figure S1). Elimination of the NH_3 molecule cis to the CBDCA moiety goes through the transition state $\mathbf{TS_{(1B\rightarrow 2A)}}$ in which the bond between the platinum center and the *cis*-NH_3 is breaking and a new bond between the carbonyl oxygen atom and the platinum center is forming.

As a consequence of this rearrangement, some hydrogen bonds are broken and new ones are formed. Structure **2A** shows the released NH_3 molecule weakly interacting, at 1.696 Å, with the other NH_3 group of carboplatin. The transition state $\mathbf{TS_{(1B\rightarrow 2A)}}$ and the minimum **2A** are calculated to be 40.8 and 26.7 kcal mol^{-1} higher in free energy relative to structure **1A**, respectively.

Along pathway 1, the reaction proceeds by a rearrangement of structure **2A**, through the transition state $\mathbf{TS_{(2A\rightarrow 2B)}}$, into the minimum structure **2B**, where the protonated COOH unit of the CBDCA moiety reorients, allowing CO_2 elimination in the subsequent step. The transition state $\mathbf{TS_{(2A\rightarrow 2B)}}$ and the **2B** minimum corresponding to the fragment ion $[\text{Carnosine} + (\text{CarbPt} - NH_3) + H]^+$, observed as the ion cluster centered

DOI: 10.1021/acs.inorgchem.5b00959
Inorg. Chem. 2015, 54, 7885−7897

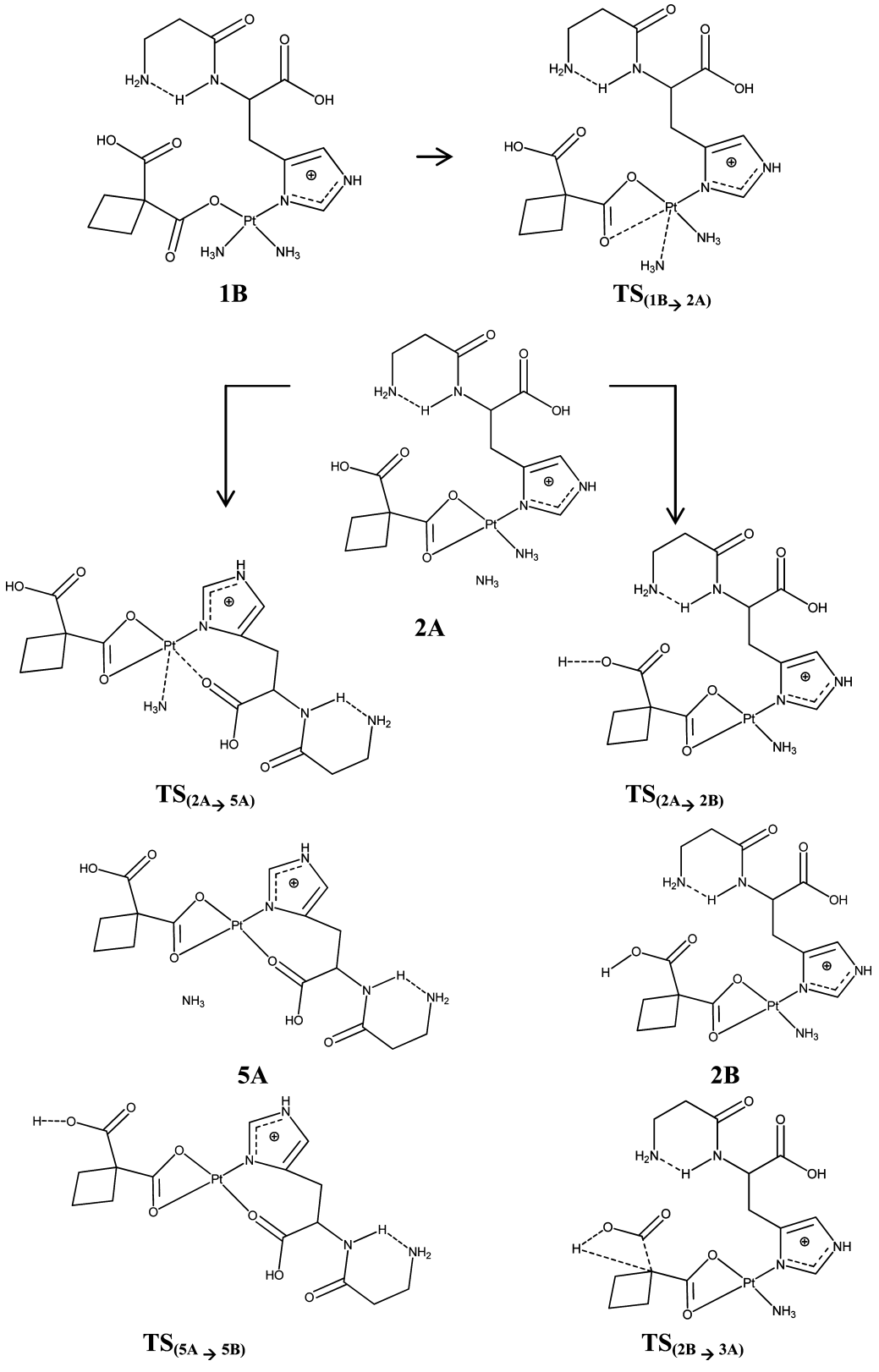

Figure 6. continued

DOI: 10.1021/acs.inorgchem.5b00959
Inorg. Chem. 2015, 54, 7885−7897

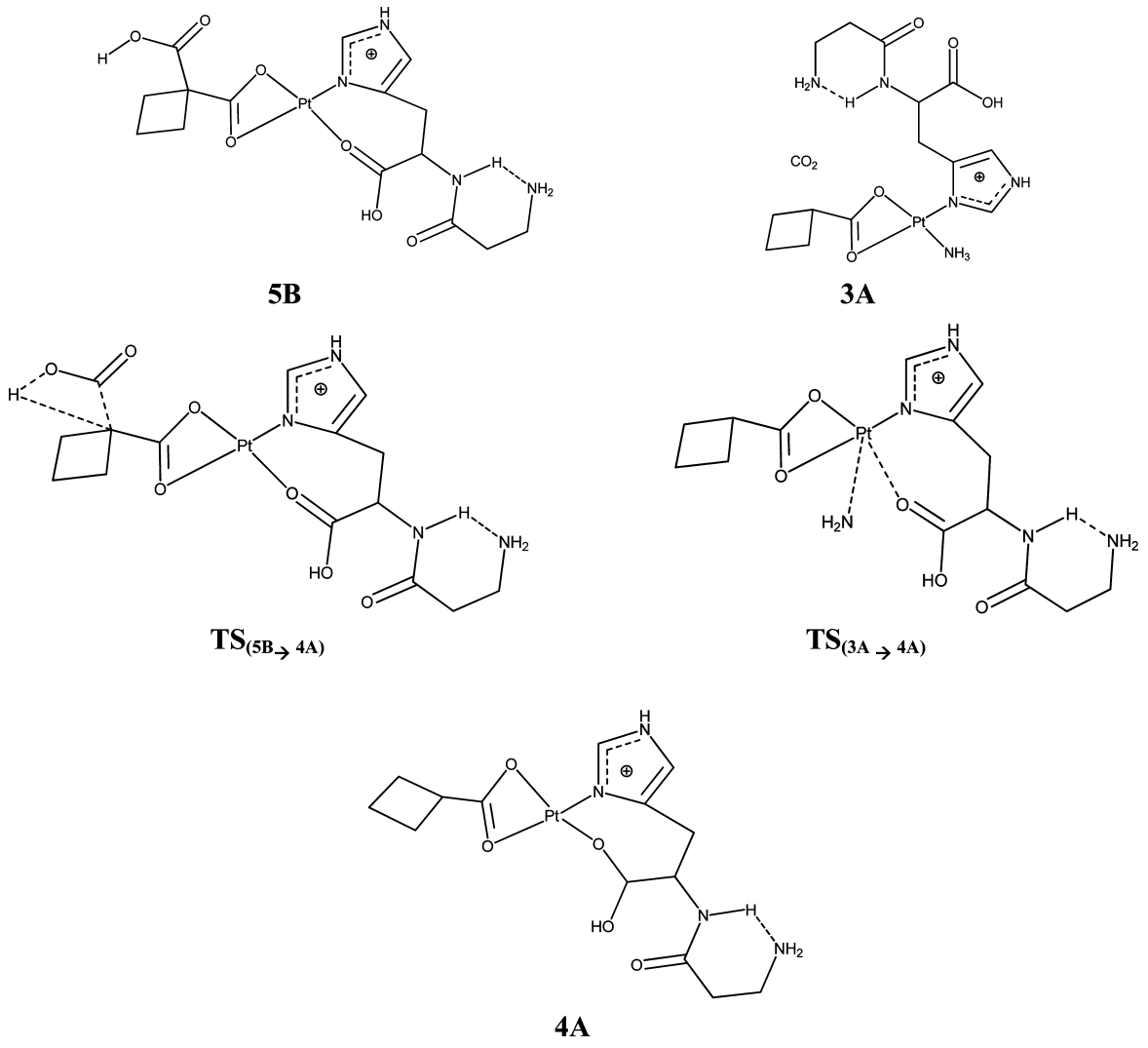

Figure 6. Schematic representation of the structures of stationary points intercepted along the fragmentation Pathways 1 and 2 for the elimination of the NH_3 molecule cis to the CBDCA ligand.

around m/z 581, are calculated to be higher in energy than the reference **1A** minimum by 39.2 and 33.8 kcal mol^{-1}, respectively. In the next step, from the protonated COOH unit of the CBDCA ligand, a CO_2 molecule is eliminated to yield the minimum **3A** corresponding to the fragment ion $[Carnosine + (CarbPt - NH_3) - CO_2 + H]^+$ observed as the ion cluster centered around m/z 537. The CO_2 loss occurs by overcoming the free-energy barrier for the transition $\mathbf{TS}_{(2B\rightarrow 3A)}$ of 101.3 kcal mol^{-1} relative to structure **1A**. In the transition $\mathbf{TS}_{(2B\rightarrow 3A)}$, the C−C bond between the COOH unit and the quaternary carbon atom of the CBDCA moiety is broken and the proton migrates from the oxygen atom of the OH group to that carbon atom, leading to the minimum structure **3A**, whose formation is endoergic by 15.0 kcal mol^{-1} relative to the starting structure **1A**. The released CO_2 appears to be bonded to the carnosine COOH group by a relatively weak hydrogen bond with a bond length of 1.797 Å. The final step of this pathway involves further elimination of the second NH_3 from the carboplatin moiety of structure **3A** to produce the fragment ion $[Carnosine + (CarbPt{-}2NH_3) - CO_2 + H]^+$ observed as the ion cluster centered around m/z 520, indicated as **4A** in Figures 5 and 6.

Similar to the first NH_3 elimination, the reaction here involves the rupture of the Pt−N bond, as shown in the transition $\mathbf{TS}_{(3A\rightarrow 4A)}$ with a barrier of 46.4 kcal mol^{-1} calculated with respect to the initial structure **1A**. This transition state describes the concerted breaking of two hydrogen bonds: the first is between the NH_3 molecule of carboplatin and the C═O moiety of the carnosine COOH group, while the second is between the OH group of COOH and the amide nitrogen atom of carnosine. The removal of these hydrogen bonds is followed by the subsequent rotation, and formation of a new bond between the carbonyl oxygen atom of the carnosine COOH and the platinum center gives the minimum structure **4A** having the released NH_3 molecule weakly attached to the remaining CBDCA carboxylate via a hydrogen bond of 2.194 Å. Structure **4A** is calculated to be 35.1 kcal mol^{-1} higher in energy relative to the zero reference energy of **1A**.

It is worth mentioning that the CO_2 molecule can be, alternatively, released from the carnosine moiety. The corresponding path, together with the structures of the intercepted stationary points, is displayed in the SI (Figure S2). After formation of the **2A** minimum, the reaction proceeds by rotation of the hydrogen atom of the OH group of the carnosine ligand to form, by overcoming a low barrier of 12.9

DOI: 10.1021/acs.inorgchem.5b00959
Inorg. Chem. 2015, 54, 7885−7897

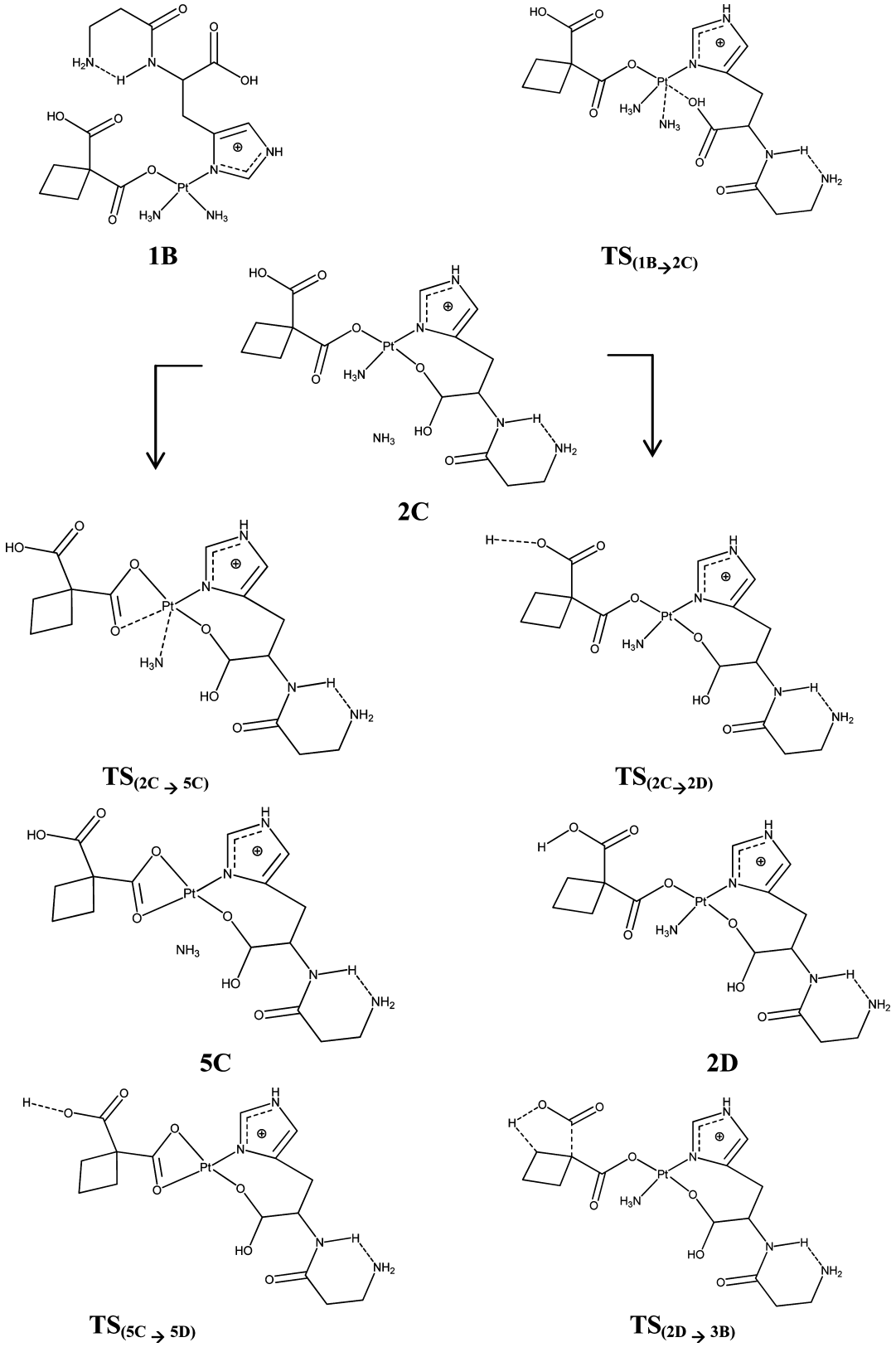

Figure 7. continued

DOI: 10.1021/acs.inorgchem.5b00959
Inorg. Chem. 2015, 54, 7885−7897

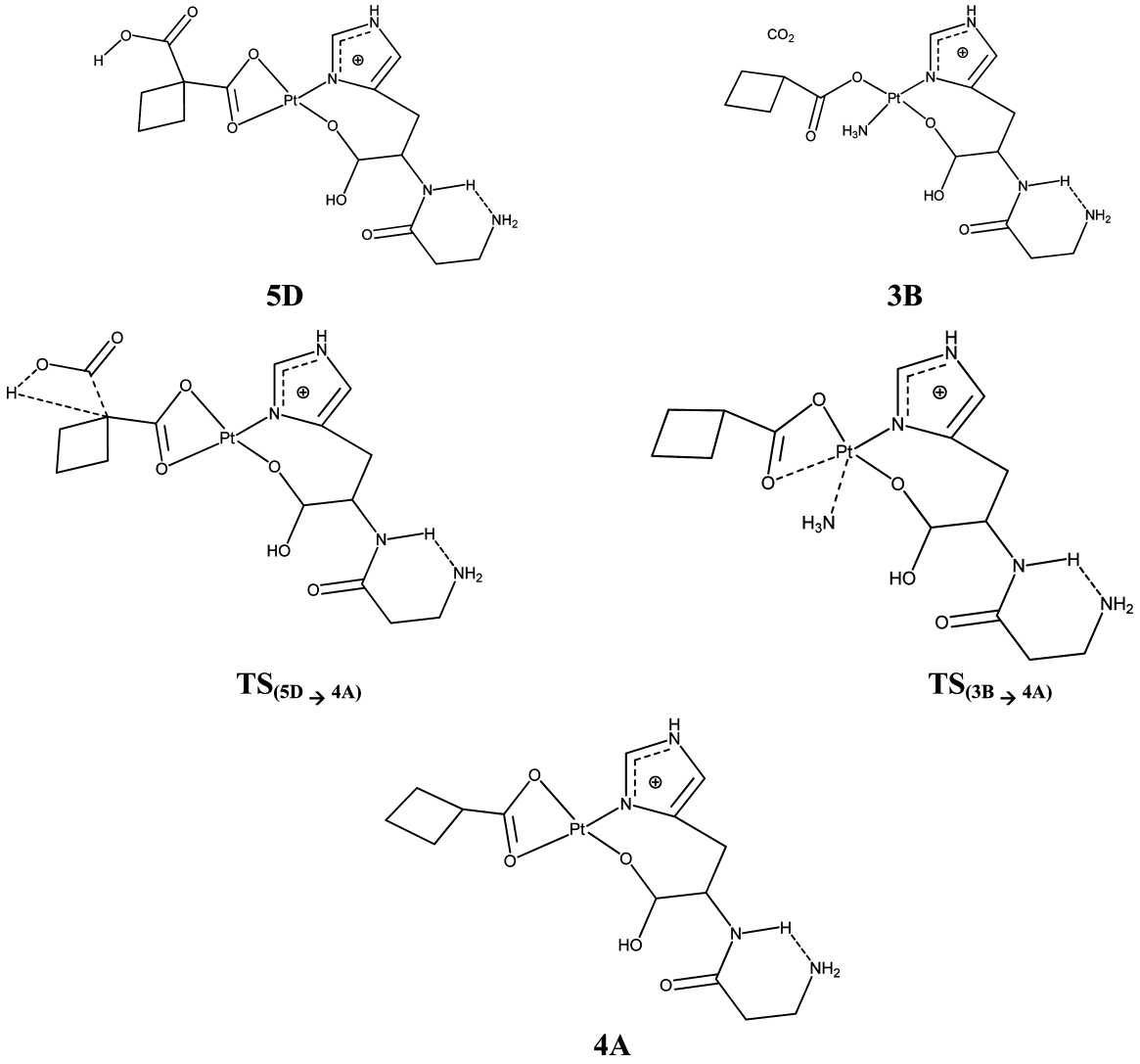

Figure 7. Schematic representation of the structures of stationary points intercepted along the fragmentation pathways 3 and 4 for elimination of the NH_3 molecule trans to the CBDCA ligand.

kcal mol^{-1} calculated with respect to the previous minimum, the intermediate labeled **2E** lying 29.8 kcal mol^{-1} above the **1A** global minimum. The transition state $\mathbf{TS}_{(2E\rightarrow 3C)}$ allows OH group hydrogen transfer to the carbon atom that releases the CO_2 molecule. This rearrangement has a high energetic cost that corresponds to an activation barrier of 112.1 kcal mol^{-1} calculated with respect to the **1A** reference energy. That is, the CO_2 loss from the COOH group of the CBDC ligand appears to be more favorable and has been examined along all of the described pathways reported below.

In contrast to pathway 1, in which elimination of the cis NH_3 molecule is followed by CO_2 loss and subsequent elimination of the second NH_3, along pathway 2, elimination of the *cis*-NH_3 molecule continues with elimination of the second carboplatin NH_3, followed by the loss of CO_2 from the CBDC COOH group. Elimination of the second ammonia from structure **2A** results in the formation of structure **5A** for the fragment ion $[\text{Carnosine} + (\text{CarbPt} - 2NH_3) + H]^+$ observed as the ion cluster centered around m/z 564. This involves breaking of the Pt−N bond, as shown in transition state $\mathbf{TS}_{(2A\rightarrow 5A)}$, being at a free-energy barrier of 71.4 kcal mol^{-1} relative to the starting structure **1A**. The formation of a bond between the carbonyl oxygen atom of the carnosine COOH group and the platinum center yields the minimum structure **5A**. The released NH_3 weakly interacts, at a distance of 1.912 Å, with the terminal amino group of carnosine. Relative to **1A**, structure **5A** is calculated to be 63.9 kcal mol^{-1} higher in energy.

Similar to the rearrangement of structure **2A** into structure **2B**, here structure **5A** internally rearranges through the transition state $\mathbf{TS}_{(5A\rightarrow 5B)}$ to form the minimum structure **5B** prior the elimination of CO_2 in the subsequent step. The stationary points $\mathbf{TS}_{(5A\rightarrow 5B)}$ and **5B** are calculated to be higher in free energy than structure **1A** by 76.6 and 70.9 kcal mol^{-1}, respectively. In analogy with the same mechanism of CO_2 loss described above for pathway 1, structure **4A** is formed upon going through the transition state $\mathbf{TS}_{(5B\rightarrow 4A)}$, where the C−C bond between the quaternary carbon atom and protonated COOH group of carboplatin is broken followed by proton transfer from the hydroxyl of the COOH group to the carbon atom, leading to the minimum structure **4A** corresponding to the fragment ion $[\text{Carnosine} + (\text{CarbPt} - 2NH_3) - CO_2 + H]^+$ observed as the ion cluster centered around m/z 520. This final transition state on this path, $\mathbf{TS}_{(5B\rightarrow 4A)}$, is calculated to be higher in free energy relative to **1A** by 121.9 kcal mol^{-1}.

Fragmentation Pathways 3 and 4: Elimination of the NH_3 Molecule Trans to the CBDCA Ligand. Structures of

DOI: 10.1021/acs.inorgchem.5b00959
Inorg. Chem. 2015, 54, 7885−7897

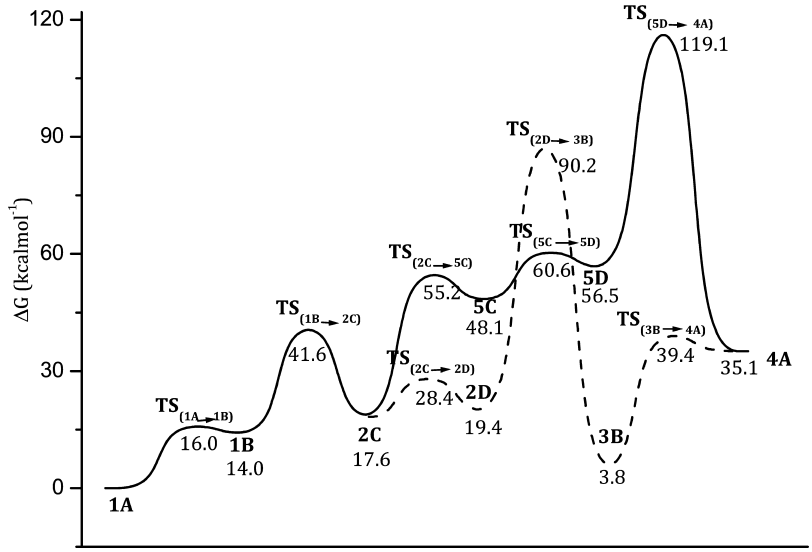

Figure 8. PES for fragmentation of the protonated carnosine−carboplatin complex, ion **1A**, along pathways 3 (solid line) and 4 (dashed line). Structure labels are in bold, and relative free energies are in kcal mol^{-1}.

all stationary points intercepted along both pathways 3 and 4 and the corresponding free-energy profiles are drawn in Figures 7 and 8. Cartesian coordinates and most relevant geometrical parameter values (Figure S3) can be found in the SI. Starting from structure **1B**, fragmentation reactions along pathways 3 and 4 involve the same initial step, which is elimination of the NH_3 molecule trans to the CBDCA moiety of carboplatin, resulting in the formation of structure **2C** corresponding to the ion [Carnosine + (CarbPt − NH_3) + H]$^+$ observed as the ion cluster centered around m/z 581. The transition state $\mathbf{TS}_{(1B\rightarrow 2C)}$ associated with elimination of the NH_3 molecule trans to the CBDCA moiety of carboplatin involves the loss of a Pt−N bond and the formation of a new bond between the carbonyl oxygen atom of the carnosine COOH group and the platinum center. The free-energy barrier of this transition state is calculated to be 41.6 kcal mol^{-1} relative to minimum **1A**. Structure **2C** formed by release of the trans NH_3 molecule is calculated to be higher than either precursor structure **1A** or **1B** in free energy by 17.6 and 3.2 kcal mol^{-1}, respectively. Structure **2C** may undergo rearrangement by rotation, so that the proton of the CBDCA COOH group is oriented toward the quaternary carbon atom of CBDCA for the CO_2 loss to occur in the next step.

This rearrangement goes through transition state $\mathbf{TS}_{(2C\rightarrow 2D)}$ as shown in pathway 3 in Figure 8, to give the minimum structure **2D**. Despite of this minor change in the structure, the transition state $\mathbf{TS}_{(2C\rightarrow 2D)}$ and the minimum **2D** are found to be 28.4 and 19.4 kcal mol^{-1} higher in free energy, respectively, relative to **1A**. Following the same mechanism of CO_2 elimination described in pathway 1, structure **2D** goes through transition state $\mathbf{TS}_{(2D\rightarrow 3B)}$, where the C−C bond is broken and the proton of the COOH group of CBDCA is transferred to the quaternary carbon atom in order to give the minimum structure **3B** corresponding to the fragment ion [Carnosine + (CarbPt − NH_3) − CO_2 + H]$^+$ observed as the ion cluster centered around m/z 537. In analogy to the other pathways previously described, CO_2 elimination here requires a high energy barrier, in this case 90.2 kcal mol^{-1} for the transition state $\mathbf{TS}_{(2D\rightarrow 3B)}$ relative to **1A**, to be overcome.

The resulting minimum structure **3B** is, however, highly stabilized and is calculated to be only 3.8 kcal mol^{-1} above structure **1A**. Finally, from structure **3B**, the remaining NH_3 molecule is released, following the same elimination mechanism in order to give structure **4A** corresponding to the fragment ion [Carnosine + (CarbPt − 2NH_3) − CO_2 + H]$^+$ observed as the ion cluster centered around m/z 520. The bond between the NH_3 nitrogen atom and the platinum center in structure **3B** is broken along with the formation of a new bond between the C═O group of the CBDCA moiety and the platinum atom in the transition state $\mathbf{TS}_{(3B\rightarrow 4A)}$ with a corresponding free-energy barrier of 39.4 kcal mol^{-1} relative to structure **1A**, leading to the formation of structure **4A**, which is 35.1 kcal mol^{-1} higher in free energy relative to **1A**.

Along pathway 4 shown in Figure 8, elimination of the first NH_3 molecule trans to CBDCA is followed by elimination of the other NH_3 molecule in order to give the minimum structure **5C** corresponding to the fragment ion [Carnosine + (CarbPt − 2NH_3) + H]$^+$ observed as the ion cluster centered around m/z 564. Elimination of the second NH_3 molecule occurs by surmounting a free-energy barrier of 55.2 kcal mol^{-1} for the transition state $\mathbf{TS}_{(2C\rightarrow 5C)}$, leading to structure **5C**, which is 48.1 kcal mol^{-1} higher in energy relative to the initial structure **1A**. That is, the minimum structure **5C** is stabilized by 7.1 kcal mol^{-1} with respect to the transition state, leading to it. Structure **5C**, in turn, rearranges so that the protonated COOH moiety of CBDCA rotates to be in a suitable orientation for CO_2 release. This is described in transition state $\mathbf{TS}_{(5C\rightarrow 5D)}$, which allows for such rearrangement and the formation of structure **5D**. These two structures are calculated to be 60.6 and 56.5 kcal mol^{-1} higher in energy with respect to **1A**, respectively. The CO_2 elimination mechanism, previously described, can then take place in which the C−C bond between the COOH group and the quaternary carbon atom of the CBDCA moiety is broken and the proton is transferred from the OH group to that carbon atom. As expected, the transition state $\mathbf{TS}_{(5D\rightarrow 4A)}$ for this transformation to finally give the minimum structure **4A** corresponding to the fragment ion [Carnosine + (CarbPt − 2NH_3) − CO_2 + H]$^+$ observed as the ion cluster centered around m/z 520 has a high energy barrier. The $\mathbf{TS}_{(5D\rightarrow 4A)}$ stationary point is calculated to be higher in free energy relative to the precursor structure **1A** by 119.1 kcal mol^{-1}.

DOI: 10.1021/acs.inorgchem.5b00959
Inorg. Chem. 2015, 54, 7885−7897

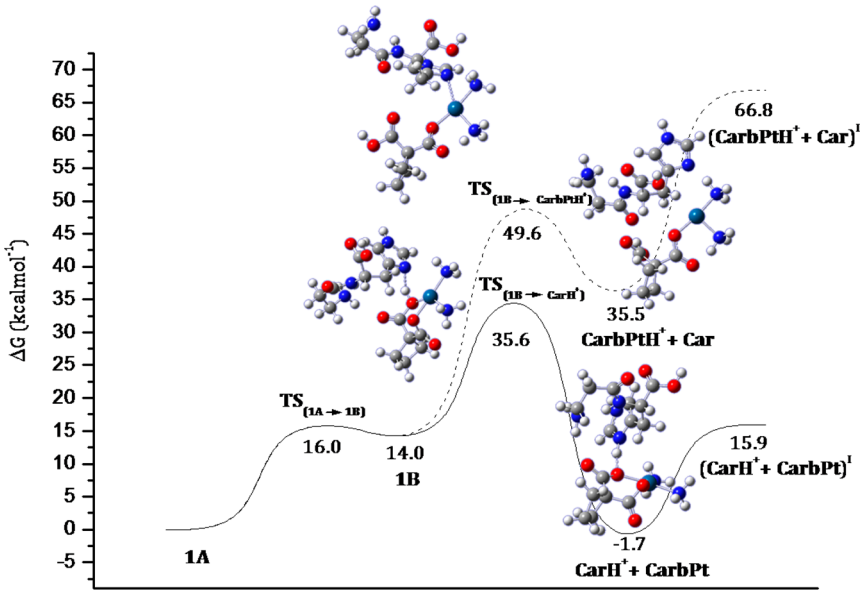

Figure 9. PES for the fragmentation of the protonated carnosine−carboplatin complex, ion **1A**, along the pathways leading to the formation of the ions $[Car + H]^+$ (solid line) and $[CarbPt + H]^+$ (dashed line). Structure labels are in bold, and relative free energies are in kcal mol^{-1}.

Production of $[CarbPt + H]^+$ and $[Carnosine + H]^+$. From the fragmentation of precursor ion $[Carnosine + CarbPt + H]^+$, it is possible to generate both $[Carnosine + H]^+$ and $[CarbPt + H]^+$ ions. The calculated pathways to produce such ions are shown in Figure 9. The structures of intercepted stationary points are depicted in the same Figure 9, whereas their Cartesian coordinates are reported in the SI. Conversion of the conformer **1A** into **1B** is followed by dissociation of the latter to produce the combinations $[Carnosine + H]^+$ and CarbPt or $[CarbPt + H]^+$ and carnosine through the transition states $\mathbf{TS}_{(1B\rightarrow CarH^+)}$ and $\mathbf{TS}_{(1B\rightarrow CarbPtH^+)}$, which present barriers of 35.6 and 49.6 kcal mol^{-1}, respectively, relative to the minimum structure **1A** reference energy. Calculated energy barriers are consistent with the experimental findings. Overcoming the concerted transition state $\mathbf{TS}_{(1B\rightarrow CarH^+)}$, in which the Pt−N bond with the imidazole ring is broken, the Pt−O bond with the carbonyl oxygen atom of the CBDCA COOH group is reestablished, and the hydrogen atom is transferred to the carnosine imidazole group, leads to formation of the combination Carnosine + H^+ and neutral carboplatin, which is calculated to be exergonic by 1.7 kcal mol^{-1} relative to structure **1A**. The final separated products, that is, the protonated carnosine fragment ion $[(Carnosine + H]^+$ observed as the ion cluster centered around m/z 227 and the neutral carboplatin complex, are, instead, less stable than the **1A** minimum by 15.9 kcal mol^{-1}. The outcomes of our computational analysis show that the fragment ion $[(Carnosine + H]^+$ production is the lowest-energy process, involving the lowest activation energy barrier calculated here. Overcoming the barrier relative to the transition state $\mathbf{TS}_{(1B\rightarrow CarbPtH^+)}$, calculated to be 49.6 kcal mol^{-1} higher in energy than structure **1A**, neutral carnosine is eliminated by breaking the Pt−N bond with the imidazole ring. The most relevant feature of the formed adduct, which is destabilized by 35.6 mol^{-1} with respect to the **1A** minimum energy, is the interaction between the T-shaped protonated carboplatin complex and the lost carnosine ligand. Indeed, the final separated products, protonated carboplatin and neutral carnosine, because of the lack of any stabilizing interaction, lie 66.8 kcal mol^{-1} above the reference energy of **1A**. A lot of attempts aimed at intercepting a different transition state and a tetracoordinated minimum have systematically failed.

4. CONCLUSIONS

DFT calculations at the B3LYP/LANL2DZ level have been carried out to describe the free-energy pathways, leading to the formation of the observed fragmentation products due to the CID of the protonated carnosine−carboplatin complex, $[Carnosine + CarbPt + H]^+$. Structural information and relative free energies for all intercepted stationary points, which account for all of the experimental findings, are reported. The most stable conformer **1A** of the $[Carnosine + CarbPt + H]^+$ complex is relatively rigid because of the presence of three internal hydrogen bonds. Consequently, the first step of all of the examined pathways is the interconversion of **1A** into a less stable and more flexible conformer **1B**. From such a precursor ion, the two combinations CarbPt and $[Carnosine + H]^+$ or Carnosine and $[CarbPt + H]^+$ can be directly produced via transition states that are calculated to be 35.5 and 49.6 kcal mol^{-1}, respectively, higher in free energy than structure **1A**. Formation of the $[Carnosine + H]^+$ ion from $[Carnosine + CarbPt + H]^+$ appears to be the lowest-energy process, as confirmed by calculations that show generation of the protonated carnosine ion and neutral carboplatin to involve the lowest energy barrier calculated here. Although not hindered by a high activation barrier, the $[CarbPt + H]^+$ ion generation is calculated to be very unfavorable from a thermodynamic point of view.

At slightly higher collision energies, the fragmentation can proceed via the loss of neutral ammonia from **1B** to give the fragment ion $[Carnosine + (CarbPt - NH_3) + H]^+$ corresponding to the observed ion cluster centered around m/z 581. Both NH_3 molecules in the cis and trans positions to the CBDCA moiety of carboplatin can be eliminated. Once elimination of the first NH_3 molecule takes place, the fragmentation process can continue with either elimination of the remaining second carboplatin NH_3 molecule, followed by the elimination of CO_2 from the COOH unit of the CBDCA moiety, or the elimination of a CO_2 molecule, followed by

DOI: 10.1021/acs.inorgchem.5b00959
Inorg. Chem. 2015, 54, 7885−7897

elimination of the second remaining NH_3 molecule of carboplatin.

■ ASSOCIATED CONTENT

Supporting Information

The Supporting Information is available free of charge on the ACS Publications website at DOI: 10.1021/acs.inorgchem.5b00959.

Geometrical structures of stationary points intercepted along all of the fragmentation pathways, free-energy profile for the CO_2 release from the carnosine ligand, and Cartesian coordinates (Å) and absolute energies (hartrees) of all optimized structures (PDF)

■ AUTHOR INFORMATION

Corresponding Authors

*E-mail: siciliae@unical.it.

*E-mail: t.shoeib@aucegypt.edu.

Notes

The authors declare no competing financial interest.

■ ACKNOWLEDGMENTS

The authors thank The American University in Cairo for funding sponsorship and the provision of resources for the project. The Dipartimento di Chimica e Tecnologie Chimiche of Università della Calabria is gratefully acknowledged.

■ REFERENCES

(1) Rosenberg, B.; Van Camp, L.; Krigas, T. *Nature* **1965**, *205*, 698−699.

(2) Rosenberg, B. In *Cisplatin. Chemistry and Biochemistry of a Leading Anticancer Drug*; Lippert, B., Ed.; Verlag Helvetica Chimica Acta: Zurich, Switzerland, 1999; Part 4, p 3.

(3) Cohen, S. M.; Lippard, S. J. *Progress in Nucleic Acids Research and Molecular Biology* **2001**, *67*, 93−130.

(4) Alderden, R. A.; Hall, M. D.; Hambley, T. W. *J. Chem. Educ.* **2006**, *83*, 728.

(5) Hambley, T. W. *Coord. Chem. Rev.* **1997**, *166*, 181−223.

(6) Wong, E.; Giandomenico, C. M. *Chem. Rev.* **1999**, *99*, 2451−2466.

(7) Boulikas, T.; Pantos, A.; Bellis, E.; Christofis, P. *Cancer Therapy* **2007**, *5*, 537−583.

(8) Reedijk, J. *Pure Appl. Chem.* **2011**, *83*, 1709−1719.

(9) Clarke, M. J.; et al. *Chem. Rev.* **1999**, *99*, 2511−2533.

(10) Peacock, A. F. A.; Sadler, P. J. *Chem. - Asian J.* **2008**, *3*, 1890−1899.

(11) Barnard, P. J.; Berners-Price, S. J. *Coord. Chem. Rev.* **2007**, *251*, 1889−1902.

(12) Bruijnincx, P. C. A.; Sadler, P. J. *Curr. Opin. Chem. Biol.* **2008**, *12*, 197−206.

(13) Monneret, C. *Ann. Pharm. Fr.* **2011**, *69*, 286−295.

(14) Kelland, L. *Nat. Rev. Cancer* **2007**, *7*, 573−584.

(15) Rose, W. C.; Schurig, J. E. *Cancer Treat. Rev.* **1985**, *12*, 1−19.

(16) Harrap, K. R. *Cancer Treat. Rev.* **1985**, *12*, 21−33.

(17) Knox, R. J.; Friedlos, F.; Lydall, D. A.; Roberts, J. J. *Cancer Res.* **1986**, *46*, 1972.

(18) Van der Vijgh, W. J. F. *Clin. Pharmacokinet.* **1991**, *21*, 242.

(19) Di Pasqua, A. J.; Goodisman, J.; Kerwood, D. J.; Toms, B. B.; Dubowy, R. L.; Dabrowiak, J. C. *Chem. Res. Toxicol.* **2006**, *19*, 139.

(20) Frey, U.; Ranford, J. D.; Sadler, P. J. *Inorg. Chem.* **1993**, *32*, 1333.

(21) Brandšteterová, E.; Kiss, F.; Chovancova, V.; Reichelova, V. *Neoplasma* **1991**, *38*, 415.

(22) Miller, S. E.; Gerard, K. J.; House, D. A. *Inorg. Chim. Acta* **1991**, *190*, 135.

(23) Jamieson, E. R.; Lippard, S. J. *Chem. Rev.* **1999**, *99*, 2467−2498.

(24) Tewey, K. M.; Chen, G. L.; Nelson, E. M.; Liu, L. F. *J. Biol. Chem.* **1984**, *259*, 9182−9187.

(25) Johnstone, T. C.; Park, G. Y.; Lippard, S. J. *Anticancer Res.* **2014**, *34*, 471−476.

(26) Gulewitsch, W.; Amiradzibi, S. *Ber. Dtsch. Chem. Ges.* **1900**, *33*, 1902−1903.

(27) Severina, I.; Bussygina, O.; Pyatakova, N. *Biochemistry-Moscow* **2000**, *65*, 783−788.

(28) Kohen, R.; Yamamoto, Y.; Cundy, K.; Ames, B. *Proc. Natl. Acad. Sci. U. S. A.* **1988**, *85*, 3175−3179.

(29) Gariballa, S. E.; Sinclair, A. J. *Age and Aging* **2000**, *29*, 207−210.

(30) Horning, M.; Blakemore, L.; Trombley, P. *Brain Res.* **2000**, *852*, 56−61.

(31) Nino, M.; Iovine, B.; Santoianni, P. *J. Cosmet., Dermatol. Sci. Appl.* **2011**, *1*, 177.

(32) Boldyrev, A. A. *Biochemistry (Mosc)* **2000**, *65*, 751−756.

(33) Guiotto, A.; Calderan, A.; Ruzza, P.; Borin, G. *Curr. Med. Chem.* **2005**, *12*, 2293−2315.

(34) Smith, E. C. *J. Physiol.* **1938**, *92*, 336−343.

(35) Baran, E. J. *Biochemistry (Mosc)* **2000**, *65*, 789−797.

(36) Nadi, N. S.; Hirsch, J. D.; Margolis, F. L. *J. Neurochem.* **1980**, *34*, 138−146.

(37) Kovacs-Nolan, J.; Mine, Y. *Animal Muscle-Based Bioactive Peptides*; Wiley-Blackwell: Hoboken, NJ, 2010; pp 225−231.

(38) Moustafa, E. M.; Camp, C. L.; Youssef, A. S.; Amleh, A.; Reid, H. J.; Sharp, B. L.; Shoeib, T. *Metallomics* **2013**, *5*, 1537−1546.

(39) Moustafa, E. M.; Ritacco, I.; Sicilia, E.; Russo, N.; Shoeib, T. *Phys. Chem. Chem. Phys.* **2015**, *17*, 12673−12682.

(40) Becke, A. D. *J. Chem. Phys.* **1993**, *98*, 5648−5652.

(41) Lee, A.; Yang, W.; Parr, R. G. *Phys. Rev. B: Condens. Matter Mater. Phys.* **1988**, *37*, 785−789.

(42) Becke, D. *Phys. Rev. A: At., Mol., Opt. Phys.* **1988**, *38*, 3098−3100.

(43) Hay, P. J.; Wadt, W. R. *J. Chem. Phys.* **1985**, *82*, 270−283.

(44) Wadt, W. R.; Hay, P. J. *J. Chem. Phys.* **1985**, *82*, 284−298.

(45) Hay, P. J.; Wadt, W. R. *J. Chem. Phys.* **1985**, *82*, 299−310.

(46) Yongye, A. B.; Giulianotti, M. A.; Nefzi, A.; Houghten, R. A.; Martinez-Mayorga, K. J. *J. Comput.-Aided Mol. Des.* **2010**, *24*, 225−235.

(47) Abdel-Ghani, N. T.; Mansour, A. M. *Eur. J. Med. Chem.* **2012**, *47*, 399−411.

(48) Wysokiński, R.; Michalska, D. *J. Comput. Chem.* **2001**, *22*, 901−912.

(49) Giese, B.; Deacon, G. B.; Kuduk-Jaworska, J.; McNaughton, D. *Biopolymers* **2002**, *67*, 294−297.

(50) Shore, T. C.; Mith, D.; DePrekel, D.; McNall, S.; Ge, Y. *React. Kinet., Mech. Catal.* **2013**, *109*, 315−333.

(51) Vacher, A.; Barrière, F.; Camerel, F.; Bergamini, J. F.; Roisnel, T.; Lorcy, D. *Dalton Trans.* **2013**, *42*, 383−394.

(52) Holmes, R. J.; O'Hair, R. A. J.; McFadyen, W. D. *Rapid Commun. Mass Spectrom.* **2000**, *14*, 2385−2392.

(53) Pazderski, L.; Tousek, J.; Sitkowski, J.; Malinakova, K.; Kozerski, L.; Szlyk, E. *Magn. Reson. Chem.* **2009**, *47*, 228−238.

(54) Moldovan, N.; Lönnecke, P.; Silaghi-Dumitrescu, I.; Silaghi-Dumitrescu, L.; Hey-Hawkins, E. *Inorg. Chem.* **2008**, *47*, 1524−1531.

(55) Moustafa, E. M.; Korany, M.; Mohamed, N. A.; Shoeib, T. *Inorg. Chim. Acta* **2014**, *421*, 123−135.

(56) Navarro, J. A. R.; Romero, M. A.; Salas, J. M.; Quiros, M.; El Bahraoui, J.; Molina, J. *Inorg. Chem.* **1996**, *35*, 7829−7835.

(57) Rajeev, R.; Sunoj, R. B. *Dalton Trans.* **2012**, *41*, 8430−8440.

(58) Ritacco, I.; Moustafa, E. M.; Sicilia, E.; Russo, N.; Shoeib, T. *Dalton Transactions* **2015**, *44*, 4455−4467.

(59) Fukui, K. *J. Phys. Chem.* **1970**, *74*, 4161−4163.

(60) Gonzalez, C.; Schlegel, H. B. *J. Chem. Phys.* **1989**, *90*, 2154−2161.

(61) Frisch, M. J.; Trucks, G. W.; Schlegel, H. B.; Scuseria, G. E.; Robb, M. A.; Cheeseman, J. R.; Scalmani, G.; Barone, V.; Mennucci, B.; Petersson, G. A.; Nakatsuji, H.; Caricato, M.; Li, X.; Hratchian, H. P.; Izmaylov, A. F.; Bloino, J.; Zheng, G.; Sonnenberg, J. L.; Hada, M.;

DOI: 10.1021/acs.inorgchem.5b00959
Inorg. Chem. 2015, 54, 7885−7897

Ehara, M.; Toyota, K.; Fukuda, R.; Hasegawa, J.; Ishida, M.; Nakajima, T.; Honda, Y.; Kitao, O.; Nakai, H.; Vreven, T.; Montgomery, J. A., Jr.; Peralta, J. E.; Ogliaro, F.; Bearpark, M.; Heyd, J. J.; Brothers, E.; Kudin, K. N.; Staroverov, V. N.; Kobayashi, R.; Normand, J.; Raghavachari, K.; Rendell, A.; Burant, J. C.; Iyengar, S. S.; Tomasi, J.; Cossi, M.; Rega, N.; Millam, J. M.; Klene, M.; Knox, J. E.; Cross, J. B.; Bakken, V.; Adamo, C.; Jaramillo, J.; Gomperts, R.; Stratmann, R. E.; Yazyev, O.; Austin, A. J.; Cammi, R.; Pomelli, C.; Ochterski, J. W.; Martin, R. L.; Morokuma, K.; Zakrzewski, V. G.; Voth, G. A.; Salvador, P.; Dannenberg, J. J.; Dapprich, S.; Daniels, A. D.; Farkas, Ö.; Foresman, J. B.; Ortiz, J. V.; Cioslowski, J.; Fox, D. J. *Gaussian 09*, revision D.01; Gaussian, Inc.: Wallingford, CT, 2009.

DOI: 10.1021/acs.inorgchem.5b00959
Inorg. Chem. 2015, 54, 7885−7897